

Lithium abundances along the RGB: FLAMES-GIRAFFE spectra of a large sample of low-mass Bulge stars[★]

T. Lebzelter¹, S. Uttenthaler^{1,★★}, M. Busso², M. Schultheis³, and B. Aringer⁴

¹ University of Vienna, Department of Astronomy, Türkenschanzstraße 17, 1180 Vienna, Austria
e-mail: thomas.lebzelter; stefan.uttenthaler@univie.ac.at

² Dipartimento di Fisica, Università di Perugia, and INFN, Sezione di Perugia. Via Pascoli, 06123 Perugia, Italy

³ Observatoire de Besançon, 41bis, avenue de l'Observatoire, 25000 Besançon, France

⁴ INAF - Padova Astronomical Observatory, Vicolo dell'Osservatorio 5, 35122, Padova, Italy

Received July 21, 2011; accepted November 07, 2011

ABSTRACT

Context. A small number of K-type giants on the red giant branch (RGB) is known to be very rich in lithium (Li). This fact is not accounted for by standard stellar evolution theory. The exact phase and mechanism of Li enrichment is still a matter of debate.

Aims. Our goal is to probe the abundance of Li along the RGB, from its base to the tip, to confine Li-rich phases that are supposed to occur on the RGB.

Methods. For this end, we obtained medium-resolution spectra with the FLAMES spectrograph at the VLT in GIRAFFE mode for a large sample of 401 low-mass RGB stars located in the Galactic bulge. The Li abundance was measured in the stars with a detectable Li 670.8 nm line by means of spectral synthesis with COMARCS model atmospheres. A new 2MASS ($J - K_S$) – T_{eff} calibration from COMARCS models is presented in the Appendix.

Results. Thirty-one stars with a detectable Li line were identified, three of which are Li-rich according to the usual criterion ($\log \epsilon(\text{Li}) > 1.5$). The stars are distributed all along the RGB, not concentrated in any particular phase of the red giant evolution (e.g. the luminosity bump or the red clump). The three Li-rich stars are clearly brighter than the luminosity bump and red clump, and do not show any signs of enhanced mass loss.

Conclusions. We conclude that the Li enrichment mechanism cannot be restricted to a clearly defined phase of the RGB evolution of low-mass stars ($M \sim 1M_{\odot}$), contrary to earlier suggestions from disk field stars.

Key words. Stars: late-type – Stars: evolution – Stars: abundances

1. Introduction

Lithium (Li) is an important diagnostic tool in stellar evolution because its abundance strongly depends on the ambient conditions. It is quickly destroyed at $T > 3 \times 10^6$ K so that it diminishes if the stellar surface is brought into contact with hot layers by mixing processes. However, if the overturn time scale for mixing becomes faster than the decay of the parent ${}^7\text{Be}$, then Li destruction reverts into production through the so-called Cameron-Fowler mechanism (Cameron & Fowler, 1971). In low-mass stars during the main-sequence phase, the initial Li abundance strongly decreases, hence slow mixing should prevail (Michaud, 1986). During the ascent on the red giant branch (RGB), any Li remaining in the envelope is further diluted by the first dredge-up (FDU); stellar models excluding atomic diffusion and rotation predict a surface Li abundance at FDU of $\log \epsilon(\text{Li}) \leq +1.5$ (where $\log \epsilon(\text{Li}) = \log[N(\text{Li})/N(\text{H})] + 12$) at this stage. This is indeed what is observed in most G-K giants (Lambert et al., 1980; Brown et al., 1989; Mishenina et al., 2006), where some of these stars show Li even far below the expectations (Mallik, 1999). However, about 1 – 2% of the K giants have a high Li

abundance and are therefore called *Li-rich* (Brown et al., 1989; de La Reza et al., 1997).

Advanced evolutionary stages in which Li abundances might possibly increase through quite fast mixing have been identified by Charbonnel & Balachandran (2000, hereafter CB00), in the moments at which the discontinuity of molecular weight μ left behind by the downward envelope expansion is erased by the advancement of the H-burning shell. This occurs at the bump of the luminosity function, which is on the RGB for low masses. For intermediate mass stars, this moment is postponed until after core He-burning, when the star climbs for the second time towards the Hayashi track and the envelope deepens again (on the so-called asymptotic giant branch, or AGB). The absence of a μ -barrier is the key factor because it allows any diffusive or plume-like mixing mechanism to link the envelope with inner layers, and in some cases does it fast enough, to activate a Cameron-Fowler mechanism for Li production. However, the proposed location of the enrichment phase directly at the RGB bump has been questioned by recent observational results (e.g. Monaco et al., 2011). Observations of Li in metal-poor globular cluster stars show that a slow extra-mixing episode at the RGB bump efficiently destroys any Li remaining after FDU (Lind et al., 2009b). Hence, evolved Li-rich stars brighter than the RGB bump are evidence that those stars somehow skip this mixing episode or even undergo a phase of Li production, which motivates the search for these stars. As it is unlikely that they skipped

[★] Based on observations at the Very Large Telescope of the European Southern Observatory, Cerro Paranal/Chile under Programme 083.D-0046(A). Table 1 is only available in electronic form at the CDS via anonymous ftp to cdsarc.u-strasbg.fr (130.79.128.5) or via <http://cdsweb.u-strasbg.fr/cgi-bin/qcat?J/A+A/>.

^{★★} The first two authors have contributed equally to this paper.

Li destruction at FDU, they must have somehow replenished it through Be decay (see the discussion in Palmerini et al., 2011).

While the Li abundance has been measured already in an increasing number of field stars (e.g. Mallik, 1999; Kumar et al., 2011; Monaco et al., 2011) the samples investigated always had the disadvantage of either inhomogeneity, especially in mass and age, uncertainty of the distance, or strong selection biases (e.g. only stars around the RGB bump). This circumstance hampers drawing definite conclusions on the evolutionary phase and length of the Li enrichment. Homogeneous samples, such as RGB stars in a cluster, are small (e.g. Pasquini et al., 2001, 2004). We therefore designed a programme to spectroscopically observe a large and homogeneous sample of stars from the bottom to the tip of the RGB belonging to the Galactic bulge (GB) to derive their Li abundances. The GB offers a large number of low-mass giants at roughly equal distance within a small area in the sky, perfectly suited for observations with a multi-object spectrograph such as FLAMES-GIRAFFE. Furthermore, in contrast to globular clusters, the Bulge contains stars in a wide range of metallicities, which provides the opportunity to check for any dependence of the Li enrichment processes on this parameter. We present the results of this programme concerning our search for Li. It will not only help to confine the phases and duration of Li production on the RGB, but will also provide a reference value for the Li abundance in the outer GB, which is needed for interpreting the first Li-rich AGB stars detected there recently (Uttenhaler et al., 2007, hereafter U07). The present data set is also of high interest for the study of the structure and nature of the bulge itself, the results of which will be presented in a forthcoming paper (Uttenhaler et al., in preparation).

2. Sample and observations

2.1. Target selection

The selection of targets was based on data from the 2MASS catalogue (Skrutskie et al., 2006) in a 25' diameter circle towards the direction $(l, b) = (0^\circ, -10^\circ)$, which is the centre of the Palomar-Groningen field no. 3 (PG3). This field in the outer GB was chosen because the sample of AGB stars studied by U07 is also located in the PG3. The GB stars in this field are roughly 1.4 kpc away from the Galactic plane and centre. A colour-magnitude diagram (CMD) to illustrate the target selection is displayed in Fig. 1. The observed targets (black circles) were chosen to fall close to two isochrones from Girardi et al. (2000), which are representative for the GB: $Z = 0.004$ and age 10×10^9 years, and $Z = 0.019$ (which is Z_\odot on the scale used by Girardi et al., 2000) and age 5×10^9 years. A distance modulus of 14^m5 to the GB was adopted. The chosen targets were allowed to have a $(J-K)_0$ colour either bracketed by the isochrones, or 0^m02 redder or bluer than these. We dereddened the stars using the linear relation for the reddening in the B_J photographic band as a function of galactic latitude given in Schultheis et al. (1998). To translate this into the extinction in the J - and K -bands, we used the relation $R = A_V/E(B-V)$ with $R = 3.2$ and the reddening law of Glass & Schultheis (2003). We find a mean reddening of 0^m129 in the J -band and 0^m049 in the K -band. A slightly higher reddening is found using the map of Schlegel et al. (1998), but the difference is within the errors of the 2MASS photometry. In addition to the selection with the colour criterion we selected only stars fainter than $J_0 = 9^m0$ to exclude AGB stars above the tip of the RGB, and stars brighter than $J_0 = 14^m5$ to include the RGB bump, which is expected from isochrones at $13^m8 \leq J_0 \leq 14^m1$. Furthermore, we discarded all targets that had fewer than two

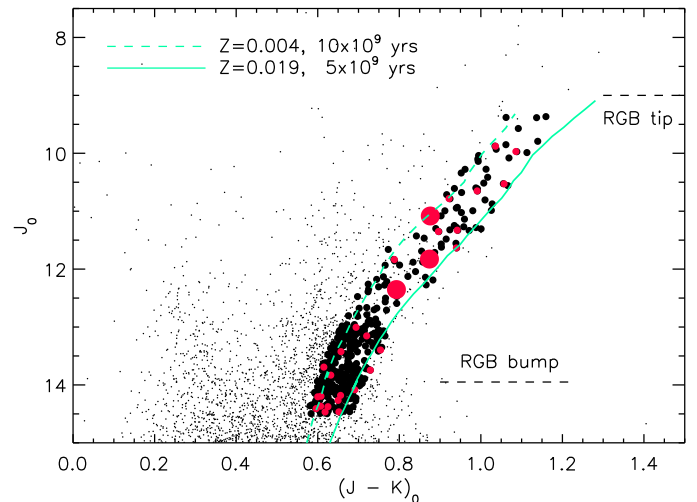


Fig. 1. 2MASS Colour-magnitude diagram of the field around $(l, b) = (0^\circ, -10^\circ)$. Stars not observed in the present programme are plotted as black dots, observed targets as black circles, stars moderately enriched in Li as small red circles, and Li-rich stars as big red circles. Two RGB isochrones from Girardi et al. (2000), with metallicities and ages as indicated in the legend, are also included. The isochrones are truncated at the tip of the RGB.

quality flags 'A' in the 2MASS JHK photometry and targets that had another source within $3''$ that was not fainter by at least 2^m0 in the J -band than the target itself. This selection scheme provides a bias against close visual pairs in our sample. Applying all those criteria yielded 514 targets for the observations.

Also discernible in Fig. 1 are the two red clumps (RCs) recently identified by Nataf et al. (2010) and McWilliam & Zoccali (2010), which probably represent two populations at different distance in the GB, which are of similar age and metallicity (De Propris et al., 2011). These structures were not known to us in the design phase of the programme. Initially, the fainter RC at $J_0 \sim 13^m9$ was interpreted by us to be the RGB bump, and only the brighter one at $J_0 \sim 13^m2$ as the red clump. This recent discovery introduces an uncertainty of a bulge star's location on the RGB of about 0^m7 . The locations of the RGB bumps of the two populations are then expected to be slightly above and below the theoretical line marked in Fig. 1. Given this range of distance moduli ($\sim 14^m1$ to $\sim 14^m8$) and the photometric errors from the 2MASS catalogue, we can estimate the expected range of metallicities in our sample with the help of the isochrones. We find that at the lower brightness end, stars down to a metallicity of $[M/H] = -1.3$ would still fall in the selection range, albeit with a lower probability than stars with a metallicity between that of the two selection isochrones. At brighter magnitudes, the lower metallicity cut will be somewhat higher, but stars down to $[M/H] = -0.7$ should be complete in the whole magnitude range of our sample. On the other hand, stars belonging to the near side of the X-shaped bulge may still fall within our selection region up to a metallicity of $[M/H] = +0.2$. As we will see in Sect. 3, a few stars fall outside this range, but those cases should be rare.

2.2. Observations and data reduction

To measure the Li abundance we obtained spectra of the sample stars using the FLAMES spectrograph in the GIRAFFE configuration. The grating HR15 centred at 665 nm was used, which

gave a spectral resolution of 17 000 for a wavelength coverage from 644 to 682 nm. This setting contains the Li resonance line at 670.8 nm and the $H\alpha$ line, in addition to several other atomic and molecular features. Because our sample stretches over a brightness range of 5 magnitudes, it was divided into three sub-groups, a bright ($11^m9 \lesssim R \lesssim 13^m3$), an intermediate ($13^m3 \lesssim R \lesssim 14^m7$), and a faint group ($14^m7 \lesssim R \lesssim 16^m2$), with total exposure times of 0.5, 1, and 4 h, respectively¹. For the bright group one fibre configuration was sufficient, while the larger number of targets at fainter magnitudes made necessary to split up the intermediate and faint group into two and three fibre configuration, respectively. The observations were obtained in service mode in June 2009. To keep observing blocks below one hour and to handle cosmic ray hits, the observations of the intermediate group were split into two, those of the faint group into five exposures. Individual spectra were extracted from each of these images separately using the FLAMES pipeline provided by ESO. The quality of each spectrum was checked, and those with low signal or cosmic ray hits in the critical wavelength ranges were rejected. Before averaging the good spectra, small wavelength shifts caused by splitting the individual observations in some cases over a few weeks were corrected. The applied shift agreed with the expected value for the difference in heliocentric correction, and the same shift was found for all spectra obtained at a given time. Therefore, we can exclude that these shifts are the result of orbital motion in a binary system. No other velocity shifts were found within the accuracy limits of our data. However, for several stars only one observation was available, therefore we point out that with the present data set an effective discrimination against binaries is not possible. We aimed at a signal-to-noise ratio (S/N) close to 100, which was achieved for most targets. Of the initially proposed sample, 401 spectra had sufficiently high quality to check for the presence of the Li line and to measure their radial velocity (RV).

2.3. Foreground contamination

An important point for this kind of study is the foreground contamination of the sample. To reliably estimate the fraction of genuine bulge stars in our sample, we ran two simulations of Galactic population models, namely the Besançon model (Robin et al., 2003) and the TRILEGAL model (Girardi et al., 2005). For the TRILEGAL simulation (kindly provided by E. Vanhollebeke), the best-fit parameters of a tri-axial bulge found by Vanhollebeke et al. (2009) were adopted. We applied the same colour and magnitude selection criteria to the simulated data as to the observed data. This selection yielded 81% and 74% bulge stars in the TRILEGAL and Besançon model, respectively. We also inspected the distribution of initial masses of the simulated stars in the selection area. The mass spectrum in the TRILEGAL simulation is relatively sharply peaked at $1.01M_{\odot}$, with a standard deviation of $0.13M_{\odot}$. Hence, we are confident that our sample indeed contains mostly low-mass ($M \sim 1M_{\odot}$) red giant stars that are located in the GB.

Some of the foreground stars might be identified by their high proper motion. We therefore searched the Southern Proper Motion Program catalogue version 4 (SPM4; Girard et al., 2011) for sample stars with high proper motion. All but ten of our sample stars were identified in the SPM4 catalogue. Unfortunately, the uncertainties in the SPM4 catalogue are large, so that bulge and foreground stars can hardly be separated. We decided to

assign those stars to the foreground whose proper motion is higher than 20 mas/yr. Applying this criterion, we found 50 foreground star candidates; these stars are marked with an asterisk in Table 1. One star in our sample (#300) has a particularly high proper motion of more than 200 mas/yr, hence it is probably a nearby K dwarf.

3. Analysis and results

For the following analysis we used hydrostatic COMARCS atmospheres in connection with the COMA spectral synthesis package (Aringer et al., 2009). This ensures a consistent treatment of radiative transfer and opacities during the complete analysis. We started with a temperature calibration based on 2MASS $(J - K_S)_0$ colours, which is presented in Appendix A. A determination of the stellar temperature and surface gravity using only the FLAMES spectra was not possible because of the limited spectral range and the dominance of TiO lines in the cooler targets. After fixing the temperature based on the colours, we obtained the surface gravities (g) from isochrones in Fig. 1 (Girardi et al., 2000), assuming that the stars belong to the Bulge RGB. The uncertainty in the distance modulus of $\pm 0^m35$ (Sect. 2) introduces an uncertainty in $\log(g)$ of ± 0.16 , which has only a very minor impact on the uncertainty in the Li abundance, however.

In a first step of the analysis of the spectra, we determined the RVs of the stars by cross-correlating the observed spectra with a synthetic spectrum that was based on a COMARCS model with a temperature close to that estimated for each star. In the next step, the observed spectra were inspected visually around the 670.8 nm Li line, together with a synthetic spectrum calculated with no Li to check for excess absorption. The Li line was found to be detectable in 31 stars. Four of these Li-bearing stars are also foreground star candidates (Sect. 2).

To estimate the metallicity of each star, we calculated model atmospheres with five different metallicities ($[M/H] = -1.5, -1.0, -0.5, 0.0, \text{ and } +0.5$), with T_{eff} and $\log g$ values determined in the previous step. A general α -element enhancement of $[\alpha/Fe] = +0.2$, a C/O ratio of 0.3, and a micro-turbulent velocity typical for red giant stars of $\xi = 2.5 \text{ km s}^{-1}$ were assumed. The spectra with the five different metallicities were interpolated and fitted to the observed spectra in the wavelength range 649 – 680 nm using the downhill simplex IDL routine amoeba.pro. The aim of this exercise was not to determine a very precise metallicity of the stars, but instead to reasonably model the quasi-continuum in the vicinity of the Li line, which is suppressed from the true continuum by a forest of weak lines, and the lines blending with the Li line. This procedure resulted in very satisfying fits of the spectra. The metallicity determined in this way is probably quite reliable, its accuracy is mainly limited by the accuracy of the temperature determination. A check of this method on the observed spectrum of Arcturus yields a metallicity of $[M/H] = -0.69$. However, if model atmospheres without an alpha-enhancement are used, this would be increased to -0.64 , which reasonably agrees with the range of metallicities found for this star in the Simbad database. We find a mean metallicity of $[M/H] = -0.48$ for the 31 Li-bearing stars, which is somewhat lower than what would be expected from previous investigations of Bulge fields close to ours (Zoccali et al., 2008)². Some of the stars have very weak metal lines, indeed. Possibly, there are selection effects introduced in the sense that the Li-rich phenomenon could be more common among metal-poor stars,

¹ The R -band limits were determined from the isochrone predictions and used in the GIRAFFE exposure time calculator.

² Performing the averaging on a *linear* scale, which is the mathematically correct way, the mean is $[M/H] = -0.21$.

and/or that the detection threshold of Li is lower at lower metallicity because of the reduced background of blending lines. Note that the three most Li-rich stars (see below) have a metallicity between -0.83 and -0.96 dex below solar.

With the stellar parameters fixed in this way, we synthesised spectra, assuming varying Li abundances to fit the observed spectra. Atomic line data for the spectral synthesis were taken from the VALD data base (Kupka et al., 1999). The line list was checked by comparing a model spectrum of Arcturus (adopting the stellar parameters and abundances found by Ryde et al., 2010) with the observed Arcturus spectrum (Hinkle et al., 2000) in the vicinity of the 671 nm Li line. Some lines present in VALD were found to be too strong in the model spectrum; their $\log(gf)$ were decreased accordingly, or the line was completely removed from the list. The abundances given in Caffau et al. (2009) were adopted as solar reference. We did not apply NLTE corrections to the Li abundances (Lind et al., 2009a) derived under LTE assumption because these corrections are usually small and, for the parameters covered by our sample stars, within the uncertainties.

The programme stars #042, #080, and #123 are identified to be Li-rich according to the classical definition, one of them (#042) has a Li abundance that agrees with the cosmic value and should be regarded as *super* Li-rich. The observed spectrum of star #042 around the Li line together with a synthetic spectrum with the best fitting abundances is displayed in Fig. 2. The spectrum of a Li-detected star (#030, $\log \epsilon(\text{Li}) = +0.1$) and of a Li-poor star (#051) are also shown in that figure. All other stars with a detected Li line have an abundance at or below the solar abundance. The error in the Li abundance was estimated by varying the stellar parameters by their uncertainty. The temperature has the highest influence on the strength of the Li line, and is uncertain by ± 160 K for the hotter stars, and ± 90 K for the cooler stars, based on the uncertainty in the 2MASS photometry. We consequently estimate an uncertainty in the Li abundance of ± 0.3 dex. Moreover, the detection threshold varies with the temperature because Li becomes more and more ionised at higher temperature. A detection threshold of $\log \epsilon(\text{Li}) = +0.5$ was derived for the hottest sample stars (4800 K), which declines to 0.0 at around 4200 K, and to ~ -0.5 at 3600 K³.

All measured Li abundances as well as important quantities of the targets are collected in Table 1. Our results are also illustrated in Fig. 1: Stars with a detected Li line are plotted as small red circles, and the Li-rich stars are plotted as large red circles.

4. Discussion

4.1. The frequency of Li rich stars

The three most Li-rich stars in our sample are located on the upper RGB, clearly above the bump and the two RCs. The faintest of our Li-rich stars (#123), at a K -magnitude of $11^m 61$, is more than one magnitude brighter than the bright RC (peak at $K \sim 12^m 65$). Taking into account the K -magnitude spread of the RCs of $0^m 22$ (David Nataf, private communication), this means that the faintest Li-rich star is brighter than the bright RC peak by 4.7 standard deviations. Hence, even considering the error in distance caused by the spread within the Bulge, it is extremely unlikely that the Li-rich stars are related to either the RGB bump or clump. On the other hand, the *Li-detected* stars are scattered all along the RGB, from below the bump to the tip. Neither at the bump nor at the RCs do we see an overdensity of Li-detected

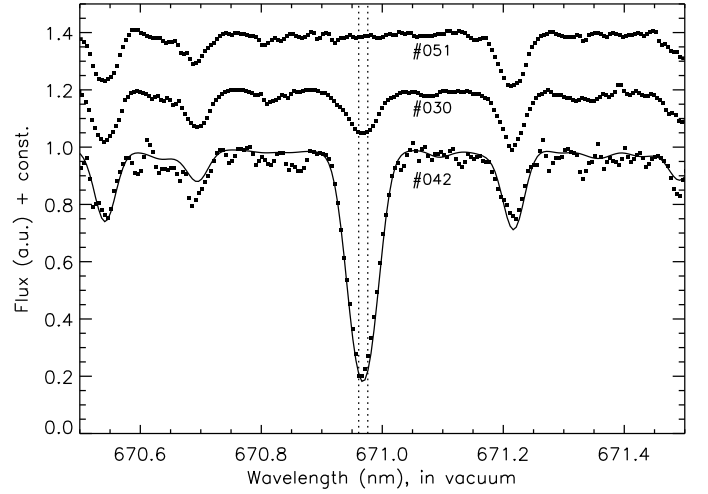


Fig. 2. Observed spectra of the programme stars #042, the most Li-rich star in our sample; #030, a Li-detected star; and #051, a Li-poor star (black dots, from bottom to top). For clarity, the spectra of stars #030 and #051 have been shifted by $+0.2$ and $+0.4$ in flux. The continuous line is the best-fit synthetic spectrum to star #042 with a Li abundance of $\log \epsilon(\text{Li}) = +3.2$. The two dotted vertical lines indicate the laboratory wavelengths of the hyperfine transitions in ^7Li . Note also the good fit to two Fe lines at ~ 670.55 and ~ 671.21 nm, which indicates a well-determined metallicity of $[\text{M}/\text{H}] = -0.85$ for star #042. The metallicities for the two other stars were determined to be -0.94 (#030) and -1.03 (#051), respectively.

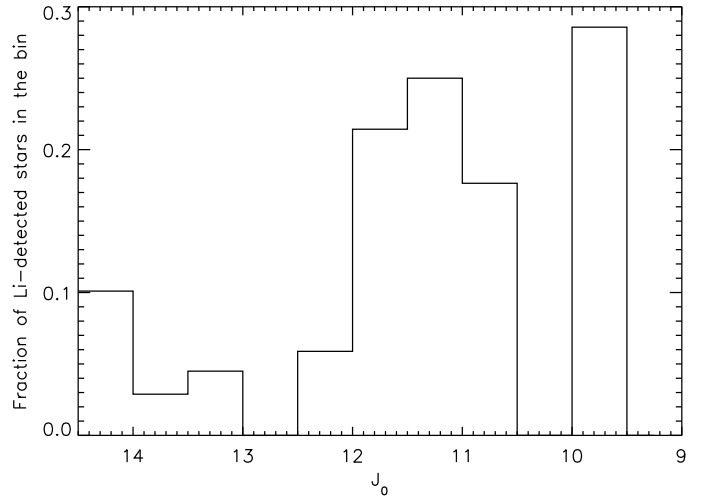


Fig. 3. Fraction of Li-detected stars as a function of J_0 .

stars. In contrast, the *fraction* of Li-detected stars on the upper RGB ($J_0 < 12^m 0$) is 18.8%, much higher than below this limit (5.4%). This important result of the present study is illustrated in Fig. 3, which shows a histogram of the fraction of Li-detected stars as a function of J_0 . The fraction of Li-detected stars also increases as a function of $(J - K_s)_0$, with a local maximum of 26.3% between $(J - K_s)_0 = 0.8$ and 0.9 .

Recently, U07 identified four AGB stars in the PG3 field with Li abundance of $\log \epsilon(\text{Li}) = 0.8, 0.8, 1.1,$ and 2.0 , among a sample of 27 long-period AGB variables. The fraction of *upper* RGB stars with detectable Li line is similar to that found among AGB stars, accordingly it is possible that the Li-rich AGB stars inherited their Li from the preceding RGB phase. Indeed, the three

³ At still lower temperatures, the detection threshold rises again because of the increasing strength of the TiO lines.

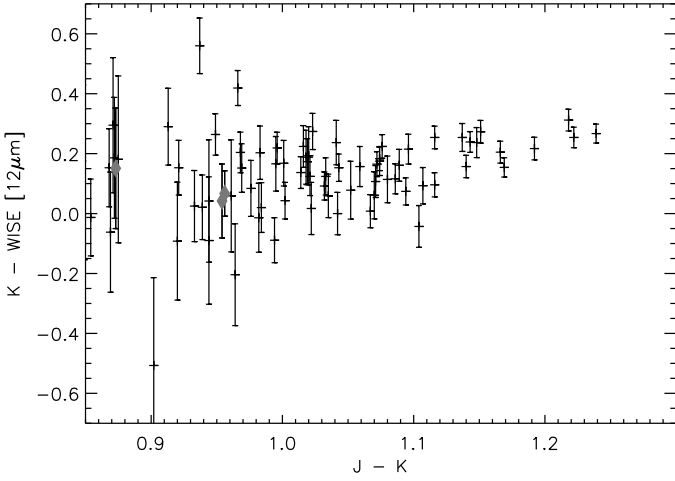


Fig. 4. $K - \text{WISE}[12\mu\text{m}]$ vs. $J - K$ colour-colour diagram of our sample stars. The grey diamond symbols represent the three Li-rich stars.

Li-rich stars identified in the present study could be early AGB stars instead of RGB stars because they are brighter than the RC. Because it is impossible to separate RGB and early AGB stars by means of our photometric and spectroscopic data alone, asteroseismological methods would be needed to better define their precise evolutionary state.

4.2. Mass loss from Li-rich stars?

It has been speculated that the Li enrichment in K-type giants is accompanied by a mass-loss episode (de La Reza et al., 1996, 1997), which has, however, later been questioned (Fekel & Watson, 1998; Jasniewicz et al., 1999). To investigate if there is enhanced *dust* mass-loss from our target stars, we cross-identified them with sources detected by the WISE space observatory (Wright et al., 2010). Within a search radius of $1''.2$ we found counterparts for 333 of our targets in the WISE catalogue⁴. We inspected $J - K$ vs. $K - \text{WISE}[3.4\mu\text{m}]$, $[4.6\mu\text{m}]$, and $[12\mu\text{m}]$ colour-colour diagrams of these stars. The $22\mu\text{m}$ WISE band proved to have too low a sensitivity to reliably detect more than just the very brightest of our targets. A version of the $J - K$ vs. $K - \text{WISE}[12\mu\text{m}]$ colour-colour diagram is displayed in Fig. 4. The x-axis range was restricted to the reddest part of the sample, because at the bluer (and hence fainter) end of the sample the noise level is very high. The few red outliers in the colour-colour diagrams were identified in the 2MASS images to be visual pairs or triples that are resolved by 2MASS, but are probably unresolved in the WISE observations. The three Li-rich stars have very inconspicuous $K - \text{WISE}$ colours, strongly suggesting that they do not suffer enhanced dusty mass-loss. For comparison, the Miras investigated by U07, which suffer a total mass-loss rate of $10^{-8} M_{\odot} \text{yr}^{-1}$ or more, have $K - [12\mu\text{m}]$ colours of 1.17 or redder.

To search also for enhanced *gas* mass-loss, we inspected the spectra of the Li-rich stars around the $H\alpha$ line in comparison with otherwise similar Li-poor stars, namely #051 and #131. Gas mass-loss would be detectable through blue-shifted asymmetries in the $H\alpha$ line profile, see e.g. Mészáros et al. (2009) for a sensitive search for gas mass-loss in red giants. The most Li-rich sample star (#042) has a slightly broader $H\alpha$ profile than the comparison stars, but no asymmetry. The other two Li-rich stars

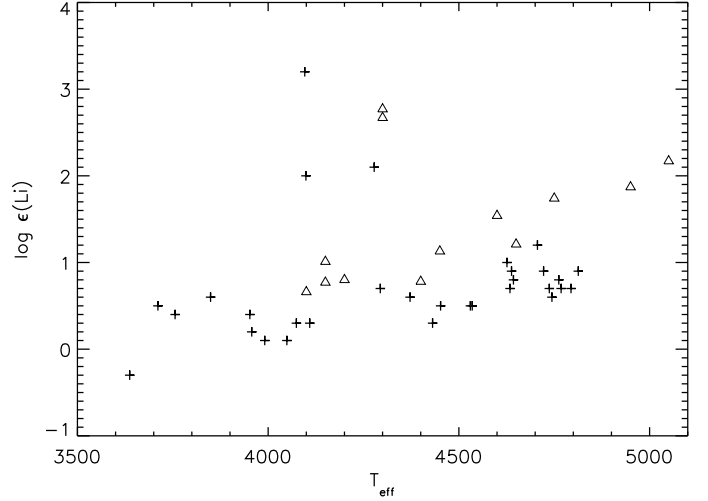


Fig. 5. Lithium abundance as a function of effective temperatures of RGB stars. The data points from our study are plotted as plus symbols, while the open triangles represent the LTE measurements from Gonzalez et al. (2009).

have a symmetric profile as well. We conclude from this that within the limits of resolution and S/N of our spectra, the Li-rich stars do not suffer enhanced loss of either dust nor gas, confirming the conclusions of Fekel & Watson (1998) and Jasniewicz et al. (1999).

4.3. A trend of Li abundance with temperature

Recently, a study of Li-rich giants in the GB was presented by Gonzalez et al. (2009). Among a sample of 417 stars, chosen from a narrow brightness range located about $0''.7$ above the expected RC, they found 13 stars with detectable Li line. Gonzalez et al. (2009) concluded that it is unlikely that the Li-rich stars are connected to either the RGB bump or the RC if they are genuine GB stars at a mean distance of 8 kpc. Although the authors' sample covers only a narrow luminosity range along the RGB, their results agree with ours. Gonzalez et al. (2009) report a decrease of the Li abundance in the Li-detected stars with decreasing temperature in their sample, which again agrees with our result. A comparison with their LTE results is presented in Fig. 5. Our sample extends the trend found by Gonzalez et al. (2009) to lower temperatures. Just as in Gonzalez et al. (2009), our Li-rich stars also deviate from this trend, and fall in a similar temperature range at $T_{\text{eff}} \approx 4100 - 4300$ K. One difference to our study is, however, that Gonzalez et al. (2009) find significantly higher Li-abundances at the hot end of their sample ($T_{\text{eff}} \geq 4600$ K) than we do. This difference is mostly caused by four stars in the Gonzalez et al. (2009) sample at $T_{\text{eff}} \geq 4600$ K and $\log \epsilon(\text{Li}) \geq 1.5$. Those stars also have a lower surface gravity ($\log g = 1.9 - 2.1$) than we estimate for our sample stars in this temperature range ($\log g = 2.3 - 2.7$). Thus, there could be a difference in evolutionary state between these groups of stars, also in terms of Li abundance, but we are not sure if this fully accounts for the found difference.

Furthermore, Gonzalez et al. (2009) also carefully examined whether the Li-rich stars are special in any other way, but did not find a difference to the Li-normal stars. In a similar attempt, we inspected the spectra of the Li-rich and Li-detected stars in our sample in comparison with Li-poor stars to search for peculiarities, but we did not find any. We only found two

⁴ <http://irsa.ipac.caltech.edu/>

sample stars with increased strength in the BaII 649.9 nm and the LaII 652.9 nm lines. They probably belong to the so-called barium star class, collecting members of binary systems that owe their enhanced s-element abundances to a mass-transfer episode from a more massive AGB companion. These will be discussed in more detail in a forthcoming paper. The Li-rich and Li-detected stars are perfectly normal in their BaII and LaII line strengths, which certifies that their Li overabundance is not the result of mass transfer of Li-enriched matter from a binary (former AGB) companion. Finally, Gonzalez et al. (2009) also conclude that their Li-rich stars do not suffer enhanced mass-loss, based 2MASS *JHK* photometry.

The three stars with the highest Li abundance in our sample fall nicely within the sequence of Li-rich thick disk giants identified by Monaco et al. (2011, their Fig. 4). Recently, Kumar et al. (2011) also identified Li-rich giants in the Galactic disk and ascribed them to the red clump, i.e. these are stars after the helium core flash. We found no accumulation of Li-rich stars close to the RCs in our sample. This could be related to a difference in mass between the stars in our study and that of Kumar et al. (2011): While there are mostly low-mass stars with a narrow distribution around $1M_{\odot}$ in our sample, the disk sample of Kumar et al. (2011) likely also contains stars of higher mass, whose Li abundance may evolve differently. The thick disk sample of Monaco et al. (2011) likely contains mostly stars of low mass as well, although the authors identify one star that could have a mass of up to $4M_{\odot}$, albeit with large uncertainty. The agreement between our results and those of Monaco et al. (2011) is probably related to a similar mass spectrum of the samples.

5. Conclusions

There are now several studies that show that at low to intermediate masses Li-rich stars can be found all along the RGB, not necessarily connected to a particular phase of the giant branch evolution (Gonzalez et al., 2009; Monaco et al., 2011; Alcalá et al., 2011; Ruchti et al., 2011). This means that either the Li enrichment process is stochastic in nature and can happen at any time on the RGB, or that Li enrichment starts at some point on the lower RGB and may take a long time to make Li-rich K giants. The activation of mixing events of variable duration and transport rates below the convective envelope is conceivable for the Li enrichment (Palmerini et al., 2011). The lack of a well-defined Li-rich phase on the RGB, as now shown by several recent studies, contradicts predictions by CB00, who propose that a Li-rich phase should occur at the bump of the RGB in low-mass stars, such as those that we have in our sample. The existence of such a Li-rich phase has to be questioned.

Acknowledgements. TL acknowledges support from the Austrian Science Fund (FWF) under projects P 21988-N16 and P 23737-N16, and SU under project P 22911-N16. BA thanks for the support from contract ASI-INAF I/009/10/0. This publication makes use of data products from the Two Micron All Sky Survey, which is a joint project of the University of Massachusetts and the Infrared Processing and Analysis Center/California Institute of Technology, funded by the National Aeronautics and Space Administration and the National Science Foundation. This publication makes use of data products from the Wide-field Infrared Survey Explorer, which is a joint project of the University of California, Los Angeles, and the Jet Propulsion Laboratory/California Institute of Technology, funded by the National Aeronautics and Space Administration.

References

Alcalá, J. M., Biazzo, K., Covino, E., Frasca, A., & Bedin, L. R., 2011, *A&A*, 531, L12
Aringer, B., 2000, Ph.D. thesis, University of Vienna, Austria

Aringer, B., Girardi, L., Nowotny, W., et al., 2009, *A&A*, 503, 913
Bessell, M. S., & Brett, J. M., 1988, *PASP*, 100, 1134
Brown, J. A., Sneden, C., Lambert, D. L., et al., 1989, *ApJS*, 71, 293
Caffau, E., Ludwig, H.-G., Steffen, M., et al., 2008, *A&A*, 488, 1031
Caffau, E., Maiorca, E., Bonifacio, P., et al., 2009, *A&A*, 498, 877
Cameron, A. G. W., & Fowler, W. A., 1971, *ApJ*, 164, 111
Carpenter, J. M., 2001, *AJ*, 121, 2851
Charbonnel, C., & Balachandran, S. C., 2000, *A&A*, 359, 563; CB00
de La Reza, R., Drake, N. A., & da Silva, L., 1996, *ApJ*, 456, L115
de La Reza, R., Drake, N. A., da Silva, L., et al., 1997, *ApJ*, 482, L77
De Propriis, R., Rich, R. M., Kunder, A., Johnson, C. I., Koch, A., et al., 2011, *ApJ*, 732, L36
Fekel, F. C., & Watson, L. C., 1998, *AJ*, 116, 2466
Girard, T. M., van Altena, W. F., Zacharias, N., Vieira, K., Casetti-Dinescu, D. I., et al., 2011, *AJ*, 142, 15
Girardi, L., Bressan, A., Bertelli, G., & Chiosi C., 2000, *A&AS*, 141, 371
Girardi, L., Groenewegen, M. A. T., Hatziminaoglou, E., & da Costa, L., 2005, *A&A*, 436, 895
Glass, I. S., & Schultheis, M., 2003, *MNRAS*, 345, 39
Gonzalez, O. A., Zoccali, M., Monaco, L., Hill, V., Cassisi, S., et al., 2009, *A&A*, 508, 289
González Hernández, J. I., & Bonifacio, P., 2009, *A&A*, 497, 497
Grevesse, N., & Sauval, A. J., 1998, *SSRv*, 85, 161
Hinkle, K., Wallace, L., Valenti, J., & Harmer, D., 2000, “Visible and Near Infrared Atlas of the Arcturus Spectrum 3727-9300 Å”, (San Francisco: ASP)
Houdashelt, M. L., Bell, R. A., Sweigart, A. V., Wing, R. F., 2000, *AJ*, 119, 1424
Jasniewicz, G., Parthasarathy, M., de Laverny, P., & Thévenin, F., 1999, *A&A*, 342, 831
Kumar, Y. B., Reddy, B. E., & Lambert, D. L., 2011, *ApJ*, 730, L12
Kupka, F., Piskunov, N., Ryabchikova, T. A., Stempels, H. C., & Weiss, W. W., 1999, *A&AS*, 138, 119
Lambert, D. L., Dominy, J. F., & Sivertsen, S., 1980, *ApJ*, 235, 114
Lind, K., Asplund, M., Barklem, P. S., 2009a, *A&A*, 503, 541
Lind, K., Primas, F., Charbonnel, C., Grundahl, F., Asplund, M., 2009b, *A&A*, 503, 545
Mallik, S. V., 1999, *A&A*, 352, 495
Marigo, P., Girardi, L., Bressan, A., 2008, *A&A*, 482, 883
Marigo, P., & Aringer, B., 2009, *A&A*, 508, 1539
McWilliam, A., & Zoccali, M., 2010, *ApJ*, 724, 1491
Mészáros, Sz., Dupree, A. K., & Szalai, T., 2009, *AJ*, 137, 4282
Michaud, G., 1986, *ApJ*, 302, 650
Mishenina, T. V., Bienaymé, O., Gorbaneva, T. I., et al., 2006, *A&A*, 456, 1109
Monaco, L., Villanova, S., Moni Bidin, C., et al., 2011, *A&A*, 529, A90
Montegriffo, P., Ferraro, F. R., Origlia, L., & Fusi Pecci, F., 1998, *MNRAS*, 297, 872
Nataf, D. M., Udalski, A., Gould, A., Fouqué, P., Stanek, K. Z., 2010, *ApJL*, 721, 28
Palmerini, S., Cristallo, S., Busso, M., Abia, C., Uttenthaler, S., et al., 2011, *ApJ*, 741, 26
Pasquini, L., Randich, S., & Pallavicini, R., 2001, *A&A*, 374, 1017
Pasquini, L., Randich, S., Zoccali, M., et al., 2004, *A&A*, 424, 951
Robin, A. C., Reylé, C., Derrière, S., et al., 2003, *A&A*, 409, 523
Ruchti, G. R., Fulbright, J. P., Wyse, R. F. G., Gilmore, G. F., Grebel, E. K., et al., accepted for publication in *ApJ*, arXiv:1111.1623
Schlegel, D. J., Finkbeiner, D. P.; Davis, M., 1998, *ApJ*, 500, 525
Ryde, N., Gustafsson, B., Edvardsson, B., et al., 2010, *A&A*, 509, A20
Schultheis, M., Ng, Y. K., Hron, J., & Kerschbaum, F., 1998, *A&A*, 338, 581
Skrutskie, M. F., Cutri, R. M., Stiening, S., et al., 2006, *AJ*, 131, 1163
Uttenthaler, S., Lebzelter, T., Palmerini, S., et al., 2007b, *A&A*, 471, L41; U07
van der Blik, N. S., Manfroid, J., & Bouchet, P., 1996, *A&AS*, 119, 547
Vanhollebeke, E., Groenewegen, M. A. T., & Girardi, L., 2009, *A&A*, 498, 95
Wright, E. L., Eisenhardt, P. R. M., Mainzer, A. K., et al., 2010, *AJ*, 140, 1868
Zoccali, M., Hill, V., Lecureur, A., et al., 2008, *A&A*, 486, 177

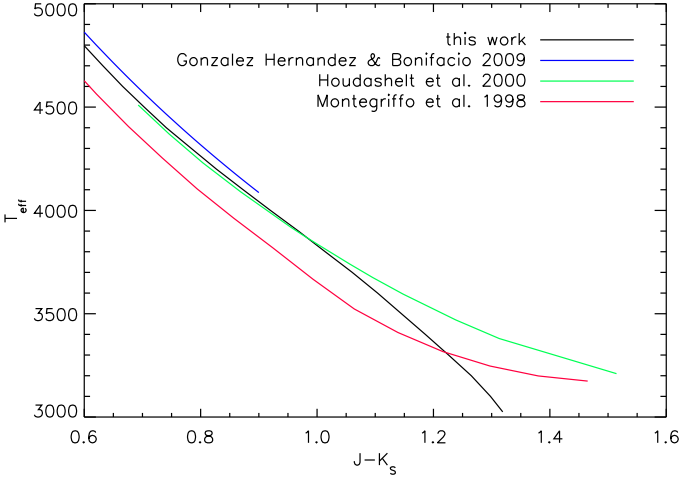


Fig. A.1. Comparison between different $(J - K_S) - T_{\text{eff}}$ calibrations as identified in the legend.

Appendix A: The $(J - K_S) - T_{\text{eff}}$ calibration from COMARCS models

In Table A.1 and Fig. A.1 we present an effective temperature calibration for the 2MASS $J - K_S$ colour based on hydrostatic COMARCS atmospheres and the COMA spectral synthesis package (see Aringer et al., 2009). The same input opacities were used for the construction of the models and the subsequent radiative transfer calculations. A list including most of the incorporated molecular species and data can be found in Marigo & Aringer (2009). The calculations are consistent with the spectral synthesis applied in this work to obtain metallicities and Li abundances.

For the presented models we assumed a microturbulent velocity of $\xi = 2.5 \text{ km s}^{-1}$, solar abundances from Grevesse & Sauval (1998), with revisions from Caffau et al. (2008, 2009) and surface gravities based on a typical solar mass and abundance evolutionary sequence (Marigo et al., 2008). Compared to the effective temperature, the influence of metallicity and surface gravity on the predicted $J - K_S$ colours is fairly small. We expect a maximum uncertainty of $\pm 50 \text{ K}$ for our programme stars owing to the variation of these quantities.

A comparison between different $(J - K_S) - T_{\text{eff}}$ calibrations is shown in Fig. A.1. Our calibration (black graph) is compared to those of González Hernández & Bonifacio (2009, blue graph), Houdashelt et al. (2000, green graph), and of Montegriffo et al. (1998, red graph). The relations of Houdashelt et al. (2000) and Montegriffo et al. (1998) were transformed from the Bessel & Brett (Bessel & Brett, 1988) and ESO (van der Bliik et al., 1996) systems, respectively, to the 2MASS system using the relations of Carpenter (2001). Solar metallicity ($[\text{Fe}/\text{H}]=0.0$) was assumed for the relation of González Hernández & Bonifacio (2009), but the dependence on metallicity is weak. This last relation is only valid up to $J - K_S = 0.9$, but an extrapolation to redder values agrees well with the other relations. The relation of Montegriffo et al. (1998) results in lower temperatures than the others by about 200 K in a broad range of $J - K_S$ values, whereas the difference between the other three relations, in the region of overlap, is small. Our relation agrees particularly well with that of Houdashelt et al. (2000) up to $J - K_S \sim 1.1$, but it subsequently diverges.

Table A.1. $(J - K_S) - T_{\text{eff}}$ calibration from COMARCS models

T_{eff}	$J - K_S$	$\log g$	BC(J)	BC(H)	BC(K)
5800	0.343	4.24	1.108	1.404	1.451
5700	0.363	4.12	1.141	1.453	1.504
5600	0.384	4.05	1.174	1.502	1.558
5500	0.407	4.01	1.205	1.552	1.612
5400	0.430	3.98	1.237	1.603	1.667
5300	0.454	3.95	1.268	1.653	1.722
5200	0.481	3.92	1.298	1.705	1.779
5100	0.509	3.88	1.327	1.757	1.836
5000	0.538	3.82	1.356	1.810	1.894
4900	0.569	3.70	1.385	1.864	1.954
4800	0.599	3.35	1.417	1.919	2.016
4700	0.632	3.03	1.447	1.973	2.079
4600	0.666	2.77	1.477	2.028	2.143
4500	0.703	2.52	1.505	2.083	2.208
4400	0.741	2.31	1.532	2.138	2.273
4300	0.784	2.11	1.557	2.193	2.341
4200	0.827	1.91	1.582	2.247	2.409
4100	0.873	1.72	1.606	2.302	2.479
4000	0.920	1.54	1.630	2.357	2.550
3900	0.968	1.35	1.656	2.412	2.624
3800	1.014	1.17	1.685	2.469	2.699
3701	1.060	1.00	1.716	2.526	2.776
3600	1.104	0.82	1.752	2.586	2.856
3500	1.145	0.67	1.792	2.646	2.937
3400	1.186	0.49	1.835	2.705	3.021
3300	1.226	0.33	1.879	2.761	3.105
3200	1.265	0.17	1.923	2.817	3.188
3100	1.298	0.03	1.966	2.873	3.264
3025	1.319	-0.11	1.998	2.912	3.317

Table 1. Parameters of the stars and measured abundances.

No.	RA(J2000) deg.	Dec(J2000) deg.	J	H	K	RV km s ⁻¹	T_{eff} K	$\log g$	[M/H]	$\log \epsilon(\text{Li})$	FG
(1)	(2)	(3)	(4)	(5)	(6)	(7)	(8)	(9)	(10)	(11)	(12)
001	276.814513	-33.589966	9.495	8.524	8.256	117.328	3465				*
002	276.544710	-33.787083	9.512	8.624	8.369	20.277	3697				
003	276.608107	-33.667065	9.516	8.615	8.298	76.484	3520				
005	276.918684	-33.751503	9.696	8.820	8.527	55.090	3629				
006	276.432104	-33.784958	9.926	9.061	8.704	-29.587	3514				
007	276.714893	-33.891556	9.978	9.096	8.838	12.913	3698				
008	276.600416	-33.681347	10.007	9.121	8.891	-135.108	3756	0.5	-0.14	0.4	
009	276.807769	-33.757442	10.057	9.178	8.941	106.494	3749				
010	276.873765	-33.726830	10.098	9.183	8.932	-128.768	3637	0.6	-0.59	-0.3	
011	276.817925	-33.649303	10.115	9.191	8.923	-59.147	3578				
012	276.611791	-33.631435	10.170	9.330	9.094	74.703	3843				
013	276.506457	-33.723846	10.213	9.322	9.062	27.664	3681				
015	276.488172	-33.844830	10.232	9.400	9.158	85.083	3847				
016	276.682337	-33.955391	10.266	9.421	9.194	25.704	3845				
017	276.595604	-33.694199	10.406	9.574	9.312	50.134	3803				
018	276.592533	-33.625336	10.409	9.579	9.366	-59.013	3914				
019	276.586978	-33.867764	10.470	9.639	9.438	178.014	3934				
020	276.704314	-33.794868	10.542	9.678	9.446	33.422	3794				*
021	276.653399	-33.955818	10.642	9.747	9.556	72.019	3815				
022	276.471245	-33.828197	10.657	9.769	9.520	-80.548	3711	0.9	+0.08	0.5	*
023	276.565931	-33.660713	10.690	9.821	9.542	-42.688	3687				
024	276.667873	-33.869152	10.726	9.949	9.659	-7.078	3857				
025	276.771326	-33.748791	10.735	9.924	9.721	-131.548	3969				
026	276.566599	-33.576355	10.747	9.916	9.673	15.044	3849				
027	276.621730	-33.925117	10.779	9.943	9.708	-0.464	3849	0.9	+0.11	0.6	
028	276.566492	-33.894100	10.807	10.005	9.774	-78.865	3932				
029	276.632910	-33.850189	10.843	10.032	9.847	305.574	4008				
030	276.876718	-33.749680	10.911	10.121	9.909	13.784	3991	1.0	-0.94	0.1	
031	276.833702	-33.646965	10.933	10.095	9.844	-12.983	3808				
032	276.664170	-33.889168	11.002	10.132	9.895	59.999	3770				
033	276.608510	-33.775723	11.064	10.240	10.041	46.289	3953				
034	276.530697	-33.808578	11.077	10.243	10.056	72.605	3959				
035	276.734398	-33.905167	11.112	10.288	10.008	37.840	3775				
036	276.693013	-33.893147	11.119	10.247	10.060	110.060	3874				
037	276.455229	-33.789265	11.126	10.329	10.132	25.919	4017				
038	276.531016	-33.587563	11.157	10.323	10.122	-105.342	3933				
039	276.476724	-33.652061	11.191	10.461	10.223	-99.668	4074	1.2	-0.17	0.3	
040	276.632713	-33.608341	11.204	10.397	10.238	-213.279	4075				
041	276.611649	-33.623035	11.212	10.433	10.228	7.052	4037				
042	276.514543	-33.867790	11.212	10.396	10.256	3.906	4096	1.2	-0.85	3.2	
043	276.545896	-33.910049	11.236	10.429	10.287	-60.971	4109	1.2	-0.61	0.3	
044	276.501519	-33.712631	11.270	10.456	10.228	-66.401	3917				
045	276.497877	-33.881786	11.378	10.535	10.362	240.911	3969				
046	276.469519	-33.651062	11.403	10.619	10.362	-1.719	3921				
047	276.718276	-33.890141	11.407	10.593	10.388	29.551	3957				
048	276.593535	-33.598366	11.415	10.584	10.345	-9.884	3857				
049	276.751404	-33.686954	11.428	10.661	10.459	81.687	4065				
050	276.668148	-33.844818	11.433	10.578	10.353	29.158	3829				
051	276.897946	-33.802887	11.446	10.612	10.445	-53.729	3992				
052	276.827522	-33.672203	11.457	10.650	10.435	-28.859	3952	1.4	+0.09	0.4	
053	276.598353	-33.763283	11.464	10.658	10.412	16.198	3893				
054	276.753347	-33.748871	11.480	10.655	10.504	21.622	4049	1.2	-0.94		
058	276.763338	-33.726757	11.555	10.775	10.634	-133.305	4167				
060	276.814847	-33.799526	11.592	10.814	10.653	19.204	4126				
061	276.745468	-33.614552	11.610	10.791	10.615	-206.421	4011				
065	276.767964	-33.723507	11.682	10.895	10.664	-59.417	3961				
067	276.764757	-33.714439	11.695	10.914	10.713	-42.029	4036				
069	276.732436	-33.691238	11.750	10.953	10.767	28.948	4035				
070	276.809016	-33.594540	11.763	10.955	10.743	-54.899	3957	1.4	-0.39	0.2	
072	276.594486	-33.730743	11.791	11.111	10.937	-52.206	4325				
073	276.836739	-33.717419	11.816	11.071	10.883	-56.535	4139				
075	276.910260	-33.767544	11.837	11.034	10.873	45.375	4070				*
080	276.663676	-33.680828	11.956	11.185	11.002	67.611	4099	1.5	-0.83	2.0	
081	276.598738	-33.673889	11.964	11.282	11.096	-155.581	4294	1.5	-0.32	0.7	
084	276.723840	-33.562702	11.989	11.339	11.120	29.832	4290				

Table 1. Continued.

No.	RA(J2000) deg.	Dec(J2000) deg.	<i>J</i>	<i>H</i>	<i>K</i>	RV km s ⁻¹	<i>T</i> _{eff} K	log <i>g</i>	[M/H]	log ϵ (Li)	FG
(1)	(2)	(3)	(4)	(5)	(6)	(7)	(8)	(9)	(10)	(11)	(12)
085	276.663499	-33.799038	12.006	11.199	11.069	58.329	4134				*
086	276.810910	-33.617214	12.009	11.269	11.096	9.035	4185				
088	276.843442	-33.804676	12.058	11.340	11.215	84.524	4343				
089	276.708411	-33.645660	12.060	11.331	11.179	-58.044	4261				
096	276.728929	-33.625156	12.172	11.457	11.252	38.482	4171				
101	276.650041	-33.653530	12.257	11.553	11.355	-123.588	4213				
102	276.603598	-33.725780	12.263	11.594	11.421	-37.926	4352				
104	276.764294	-33.611069	12.270	11.528	11.326	23.454	4119				
107	276.796933	-33.752850	12.304	11.596	11.481	16.073	4392				
108	276.818554	-33.721001	12.315	11.546	11.354	-55.377	4080				
110	276.831116	-33.661152	12.343	11.625	11.495	-109.396	4334				
112	276.844085	-33.719276	12.386	11.681	11.584	-3.301	4444				
115	276.876631	-33.669006	12.398	11.613	11.454	-172.477	4115	1.7	-0.56	< -0.3	
116	276.886129	-33.817890	12.401	11.716	11.560	-54.145	4346				*
117	276.839217	-33.735954	12.407	11.626	11.535	-141.307	4277				
118	276.605428	-33.607613	12.438	11.750	11.607	31.103	4380	1.7	-1.19	< -0.3	
121	276.850407	-33.727764	12.470	11.850	11.667	-2.194	4441				
123	276.733228	-33.686802	12.482	11.722	11.609	-85.450	4278	1.7	-0.96	2.1	
128	276.674814	-33.794342	12.520	11.823	11.717	32.514	4446				
131	276.862902	-33.842964	12.596	11.871	11.725	-28.810	4277				
132	276.529376	-33.635666	12.607	11.953	11.827	-159.866	4514				
133	276.754996	-33.640835	12.630	11.933	11.784	136.734	4341				*
136	276.670396	-33.678337	12.694	11.991	11.848	-16.510	4342				
139	276.669257	-33.560745	12.724	12.024	11.849	-8.143	4278				
142	276.592785	-33.609268	12.796	12.171	11.994	-120.627	4454				
143	276.720586	-33.791100	12.801	12.219	11.977	-28.694	4391				*
144	276.724865	-33.593685	12.806	12.156	12.024	47.662	4504				
147	276.605327	-33.599644	12.834	12.130	12.014	-13.128	4407				
148	276.808190	-33.749828	12.835	12.127	11.988	-40.138	4335				
154	276.884497	-33.711712	12.903	12.231	12.130	-74.863	4521				
156	276.802245	-33.615543	12.915	12.209	12.115	5.379	4453				*
158	276.607949	-33.626446	12.936	12.308	12.179	47.731	4574				
159	276.506642	-33.859463	12.947	12.320	12.168	-67.344	4514				
167	276.696311	-33.687943	12.992	12.354	12.170	16.036	4398				
169	276.585971	-33.583626	13.016	12.356	12.206	-21.109	4434				
172	276.674085	-33.722809	13.036	12.399	12.232	62.310	4444				
178	276.673132	-33.740860	13.069	12.451	12.242	-14.891	4385				
180	276.715472	-33.633411	13.078	12.449	12.266	57.926	4424				*
182	276.772886	-33.712326	13.085	12.412	12.316	-44.163	4535				
183	276.791120	-33.629635	13.088	12.478	12.337	-74.273	4584				
184	276.841313	-33.728474	13.093	12.437	12.271	13.471	4393				
186	276.721044	-33.780018	13.110	12.489	12.371	29.773	4618				
187	276.533345	-33.873089	13.112	12.435	12.314	-142.788	4462				
188	276.753476	-33.945801	13.119	12.543	12.370	19.007	4585				
190	276.538801	-33.644936	13.134	12.484	12.360	11.192	4530	2.1	+0.27	0.5	
191	276.627097	-33.841202	13.146	12.522	12.389	-175.576	4569				
192	276.790756	-33.846645	13.151	12.493	12.363	-8.106	4481				
193	276.717695	-33.835640	13.153	12.548	12.410	56.213	4605				
194	276.864580	-33.723576	13.154	12.547	12.417	-33.430	4620				
195	276.694217	-33.601109	13.163	12.508	12.393	-3.184	4537				
196	276.841761	-33.689163	13.167	12.539	12.385	-44.337	4499				*
197	276.749744	-33.856068	13.171	12.572	12.406	-22.102	4544				
198	276.638867	-33.930489	13.179	12.505	12.351	89.036	4381				
199	276.601595	-33.643906	13.190	12.594	12.394	55.281	4469				
200	276.910018	-33.774948	13.190	12.585	12.420	-23.265	4527				
201	276.655418	-33.667728	13.192	12.617	12.458	-12.106	4637				
202	276.600953	-33.920620	13.193	12.561	12.403	-72.007	4480				
203	276.718361	-33.917198	13.194	12.505	12.362	-112.531	4370				
204	276.651481	-33.734238	13.196	12.496	12.354	-44.013	4351				
205	276.778831	-33.720421	13.203	12.613	12.452	-66.094	4583				
206	276.529719	-33.594994	13.210	12.613	12.466	26.825	4613				
207	276.854131	-33.731907	13.221	12.595	12.447	62.408	4519				
208	276.628729	-33.743752	13.226	12.621	12.494	-39.333	4642				
209	276.798530	-33.662918	13.233	12.540	12.415	95.619	4405				
210	276.836967	-33.769405	13.243	12.643	12.456	21.124	4484				

Table 1. Continued.

No.	RA(J2000) deg.	Dec(J2000) deg.	<i>J</i>	<i>H</i>	<i>K</i>	RV km s ⁻¹	<i>T</i> _{eff} K	log <i>g</i>	[M/H]	log ϵ (Li)	FG
(1)	(2)	(3)	(4)	(5)	(6)	(7)	(8)	(9)	(10)	(11)	(12)
211	276.756279	-33.788357	13.248	12.575	12.430	-34.348	4404				
212	276.892143	-33.753590	13.248	12.670	12.487	21.790	4552				*
215	276.537753	-33.603622	13.256	12.649	12.491	-119.873	4555				*
216	276.630558	-33.724087	13.258	12.652	12.484	38.871	4526				
217	276.611185	-33.719536	13.258	12.650	12.506	53.834	4586				
218	276.533293	-33.793808	13.263	12.630	12.449	25.411	4421				
219	276.490017	-33.791950	13.267	12.645	12.524	70.196	4614				
220	276.786346	-33.598869	13.267	12.685	12.496	36.370	4531				*
221	276.488605	-33.676846	13.277	12.662	12.508	-68.765	4544				
222	276.765113	-33.566185	13.280	12.582	12.447	89.637	4371				
223	276.689571	-33.850536	13.283	12.596	12.483	63.721	4452	2.1	-0.01	0.5	
224	276.530160	-33.772533	13.283	12.630	12.546	-159.749	4630				*
225	276.490013	-33.854095	13.287	12.654	12.528	-2.227	4568				
226	276.441487	-33.833378	13.287	12.601	12.440	86.733	4344				
227	276.460830	-33.865948	13.295	12.693	12.545	-30.132	4593				
228	276.567606	-33.881664	13.305	12.729	12.573	5.293	4641				
229	276.488238	-33.744823	13.308	12.659	12.507	-93.491	4457				
230	276.701957	-33.724052	13.317	12.670	12.492	-15.167	4390				*
231	276.521504	-33.882675	13.318	12.634	12.517	87.725	4454				
232	276.701163	-33.812206	13.321	12.791	12.593	46.717	4650				
233	276.742927	-33.655430	13.327	12.768	12.577	-33.817	4588				
234	276.817331	-33.599476	13.328	12.681	12.582	3.010	4598				
235	276.561797	-33.754608	13.331	12.760	12.590	2.381	4618				
236	276.811041	-33.747356	13.339	12.698	12.552	-36.405	4485				*
237	276.543824	-33.638008	13.349	12.771	12.601	-128.142	4601				
238	276.707179	-33.863255	13.363	12.721	12.560	-48.485	4443				
239	276.514484	-33.893902	13.367	12.706	12.596	-6.349	4534				
240	276.494178	-33.865170	13.374	12.671	12.545	-45.410	4384				
241	276.691228	-33.652210	13.381	12.740	12.621	163.130	4563				
242	276.769980	-33.622349	13.400	12.785	12.587	37.049	4420				
243	276.445539	-33.820004	13.401	12.802	12.662	-201.762	4626				*
245	276.458400	-33.680145	13.410	12.870	12.674	-0.726	4637				
246	276.732205	-33.735016	13.413	12.722	12.633	-20.965	4506				
247	276.652760	-33.666142	13.415	12.859	12.647	-12.734	4542				
248	276.663722	-33.563961	13.423	12.782	12.703	-91.605	4680				
249	276.874535	-33.706005	13.432	12.805	12.675	20.002	4564				
251	276.814218	-33.891129	13.436	12.813	12.703	-100.233	4630				
252	276.590433	-33.824047	13.447	12.815	12.625	14.280	4399				
253	276.698884	-33.720577	13.450	12.802	12.707	-12.354	4608				
254	276.560443	-33.786304	13.457	12.905	12.659	47.473	4463				
256	276.885368	-33.847267	13.459	12.843	12.729	47.665	4637				
257	276.673226	-33.739399	13.464	12.896	12.744	53.227	4676				
258	276.509126	-33.638287	13.466	12.795	12.648	20.249	4414				
259	276.903426	-33.794418	13.475	12.812	12.641	0.338	4362				
260	276.856050	-33.636570	13.477	12.791	12.647	-99.944	4375				
261	276.597652	-33.706051	13.478	12.889	12.705	-56.387	4530				
262	276.627210	-33.776421	13.481	12.854	12.717	-31.979	4552				
263	276.659752	-33.951805	13.489	12.884	12.727	-5.578	4553				
264	276.545369	-33.932869	13.493	12.880	12.781	-61.467	4701				
266	276.533760	-33.787659	13.505	12.874	12.744	-68.790	4562				
267	276.616984	-33.586750	13.506	12.954	12.792	-101.202	4699				
268	276.494876	-33.647800	13.515	12.919	12.794	71.564	4681				*
269	276.764459	-33.589680	13.518	12.940	12.784	69.289	4635				
270	276.614926	-33.938892	13.526	12.948	12.808	65.396	4680				
271	276.465499	-33.869881	13.526	12.857	12.692	29.413	4372	2.3	+0.48	0.6	
272	276.827432	-33.753338	13.529	12.833	12.770	-104.732	4559				
273	276.785331	-33.659843	13.538	12.873	12.710	223.568	4381				
274	276.842104	-33.732456	13.541	12.852	12.714	-21.443	4381				
275	276.765440	-33.581825	13.554	12.999	12.817	68.660	4626	2.3	-0.76	1.0	
276	276.728640	-33.949757	13.557	12.951	12.756	-121.711	4446				
277	276.505794	-33.774723	13.561	12.941	12.782	-51.159	4515				
278	276.714377	-33.724106	13.581	13.007	12.860	16.094	4672				
279	276.619384	-33.610786	13.591	12.968	12.842	50.290	4596				
280	276.699742	-33.801800	13.600	13.064	12.896	-22.286	4722				
281	276.632739	-33.920406	13.601	12.931	12.843	-74.670	4565				

Table 1. Continued.

No.	RA(J2000) deg.	Dec(J2000) deg.	<i>J</i>	<i>H</i>	<i>K</i>	RV km s ⁻¹	<i>T</i> _{eff} K	log <i>g</i>	[M/H]	log ϵ (Li)	FG
(1)	(2)	(3)	(4)	(5)	(6)	(7)	(8)	(9)	(10)	(11)	(12)
282	276.603736	-33.792931	13.606	13.010	12.886	-59.064	4678				
283	276.839527	-33.652874	13.614	12.951	12.909	-47.148	4717				*
284	276.724473	-33.882050	13.619	12.995	12.858	-6.884	4555				
285	276.810256	-33.899017	13.632	12.985	12.875	24.234	4562				*
286	276.629095	-33.587997	13.646	13.024	12.914	-104.407	4645				
287	276.860156	-33.865948	13.646	13.033	12.895	75.530	4578				
288	276.589341	-33.604183	13.659	13.078	12.939	-63.114	4682				
291	276.787583	-33.871380	13.673	13.065	12.954	-22.181	4673				
292	276.501441	-33.769341	13.689	13.075	12.971	-60.436	4688				
294	276.807204	-33.744389	13.705	13.002	12.912	-92.853	4469				
295	276.671937	-33.722317	13.712	13.142	13.001	-7.833	4704				
296	276.472514	-33.777775	13.719	13.094	12.963	121.918	4578				
297	276.686566	-33.655930	13.744	13.148	13.021	-110.334	4669				
298	276.665050	-33.818905	13.746	13.132	13.029	87.153	4684				
299	276.859868	-33.871136	13.748	13.085	12.995	-105.991	4572				
300	276.442637	-33.752930	13.750	13.103	13.048	-23.401	4737				*
301	276.695536	-33.764545	13.751	13.160	13.029	-68.258	4669				
302	276.749584	-33.841690	13.752	13.130	13.059	-165.133	4752				
304	276.677892	-33.890118	13.758	13.194	12.984	54.041	4521				
305	276.676672	-33.567745	13.771	13.127	13.063	-54.614	4715				
306	276.686629	-33.707558	13.777	13.146	13.024	-57.854	4581				
307	276.712714	-33.944599	13.782	13.237	13.092	-73.813	4760				*
308	276.542295	-33.749485	13.790	13.240	13.092	-103.250	4746				
309	276.845057	-33.643093	13.797	13.196	13.031	-7.766	4542				
310	276.737301	-33.623081	13.801	13.204	13.097	68.140	4724				
311	276.855065	-33.892948	13.813	13.230	13.106	-10.062	4706				
312	276.805007	-33.749069	13.817	13.247	13.105	-18.932	4695				
313	276.803927	-33.834248	13.821	13.261	13.126	29.782	4744	2.4	-0.71	0.6	*
314	276.622601	-33.794971	13.822	13.150	13.024	-60.428	4460				
315	276.821083	-33.773975	13.822	13.218	13.084	96.113	4618				*
316	276.689193	-33.710064	13.845	13.207	13.090	0.896	4575				*
317	276.527656	-33.798317	13.846	13.287	13.138	-20.465	4716				
318	276.605035	-33.901566	13.846	13.198	13.094	-8.413	4583				
319	276.676819	-33.581738	13.852	13.225	13.053	-58.955	4460				
320	276.826131	-33.769146	13.853	13.137	13.051	-41.389	4444				*
321	276.547129	-33.646622	13.857	13.271	13.155	11.187	4736				
322	276.625298	-33.608067	13.858	13.294	13.140	-54.255	4687				
323	276.850420	-33.753113	13.859	13.172	13.081	-52.017	4508				*
324	276.648919	-33.838467	13.868	13.295	13.114	29.848	4577				*
325	276.887809	-33.831329	13.871	13.297	13.117	-84.110	4569				*
326	276.520313	-33.606983	13.871	13.248	13.174	-13.705	4753				
327	276.743296	-33.606194	13.874	13.244	13.065	20.670	4431	2.5	-0.31	0.3	
328	276.748212	-33.826157	13.875	13.305	13.185	-29.200	4761				
329	276.494197	-33.811489	13.876	13.340	13.159	10.821	4690				
330	276.905290	-33.690044	13.879	13.243	13.114	-21.543	4542				
331	276.661029	-33.805126	13.882	13.245	13.169	-85.801	4696				
332	276.725178	-33.922646	13.894	13.301	13.118	74.659	4514				
333	276.803651	-33.785221	13.895	13.274	13.161	-160.010	4630				
334	276.573211	-33.613113	13.897	13.384	13.189	30.030	4718				*
335	276.754422	-33.812862	13.899	13.284	13.177	-3.150	4666				
336	276.775634	-33.868172	13.902	13.205	13.179	-19.149	4661				*
337	276.609719	-33.899956	13.910	13.284	13.186	86.522	4663				
338	276.802770	-33.607288	13.910	13.270	13.182	-31.855	4651				*
339	276.599163	-33.751358	13.916	13.369	13.197	21.543	4682				
340	276.862496	-33.881008	13.916	13.287	13.203	-7.419	4688				
342	276.619675	-33.905045	13.925	13.343	13.216	123.234	4708				
343	276.694856	-33.562214	13.926	13.257	13.149	69.723	4519				
344	276.586781	-33.832466	13.931	13.301	13.158	214.266	4528				
347	276.736184	-33.875690	13.949	13.316	13.213	-45.041	4624				
348	276.578552	-33.619892	13.950	13.352	13.202	5.935	4600				
349	276.737919	-33.695145	13.956	13.350	13.207	-65.841	4590				
350	276.456610	-33.796585	13.957	13.347	13.225	-120.618	4647				
351	276.564966	-33.635128	13.960	13.423	13.248	128.623	4706	2.5	+0.17	1.2	
353	276.861593	-33.801018	13.974	13.438	13.274	22.706	4728				
354	276.722013	-33.592499	13.974	13.376	13.238	46.922	4630				

Table 1. Continued.

No.	RA(J2000) deg.	Dec(J2000) deg.	<i>J</i>	<i>H</i>	<i>K</i>	RV km s ⁻¹	<i>T</i> _{eff} K	log <i>g</i>	[M/H]	log ϵ (Li)	FG
(1)	(2)	(3)	(4)	(5)	(6)	(7)	(8)	(9)	(10)	(11)	(12)
355	276.749304	-33.665966	13.975	13.357	13.210	-58.417	4547				
356	276.762247	-33.786091	13.982	13.460	13.272	20.393	4702				
357	276.785991	-33.896404	13.985	13.341	13.224	-84.393	4553				
358	276.833052	-33.776608	13.989	13.368	13.235	-0.947	4572				
359	276.433122	-33.740566	13.989	13.411	13.292	-32.267	4753				
360	276.691675	-33.846764	13.993	13.347	13.275	-38.991	4679				
361	276.705482	-33.740154	13.996	13.411	13.280	37.993	4687				
362	276.617111	-33.760021	13.996	13.410	13.278	7.110	4684				
363	276.493794	-33.799362	13.996	13.417	13.299	30.066	4750				
364	276.697108	-33.596195	13.996	13.460	13.297	49.761	4741				
365	276.575708	-33.577957	14.000	13.428	13.271	0.930	4656				
366	276.663677	-33.647522	14.002	13.400	13.306	12.679	4750				
367	276.779362	-33.567799	14.002	13.382	13.217	188.004	4495				
368	276.871279	-33.792786	14.006	13.428	13.318	-35.508	4764				
369	276.580553	-33.632629	14.007	13.438	13.271	-80.578	4634				
370	276.711834	-33.703365	14.013	13.394	13.306	48.722	4714				
371	276.743577	-33.898552	14.014	13.444	13.263	-93.685	4581				*
373	276.441719	-33.814545	14.024	13.424	13.276	2.274	4601				
374	276.570897	-33.627617	14.025	13.431	13.228	-16.193	4468				
376	276.747908	-33.773846	14.027	13.360	13.322	-31.917	4718				
377	276.641959	-33.642696	14.027	13.439	13.293	9.039	4638				*
378	276.686341	-33.926971	14.032	13.484	13.341	119.348	4758				
379	276.867112	-33.799599	14.035	13.406	13.344	36.952	4755				
380	276.797940	-33.867813	14.041	13.329	13.276	10.755	4542				
381	276.615896	-33.679054	14.044	13.455	13.337	-41.469	4718				
382	276.642599	-33.707905	14.051	13.414	13.319	29.732	4642				*
383	276.552809	-33.793800	14.052	13.441	13.273	58.636	4514				
384	276.767664	-33.790257	14.054	13.476	13.288	-40.420	4542				
385	276.519644	-33.920509	14.060	13.538	13.278	-29.684	4504				*
386	276.778487	-33.904800	14.063	13.482	13.386	7.124	4799				*
387	276.738181	-33.939156	14.068	13.462	13.390	93.169	4797				*
388	276.529173	-33.642719	14.071	13.505	13.331	-107.163	4624				
389	276.805911	-33.751480	14.078	13.399	13.380	179.763	4737				*
390	276.654480	-33.594334	14.081	13.422	13.341	-8.853	4621				
392	276.628139	-33.834789	14.097	13.540	13.394	7.430	4726				*
393	276.710695	-33.846008	14.100	13.400	13.312	84.567	4484				
394	276.689541	-33.778378	14.107	13.531	13.367	28.170	4616				
395	276.514699	-33.757675	14.110	13.464	13.352	143.624	4572				
396	276.694978	-33.943527	14.117	13.546	13.403	90.426	4689				
397	276.828208	-33.699005	14.118	13.473	13.418	31.582	4731				
398	276.515313	-33.784389	14.119	13.550	13.332	-78.551	4493				
399	276.634575	-33.901833	14.126	13.579	13.433	-52.671	4755				
400	276.829987	-33.806454	14.127	13.557	13.385	-47.000	4605				
401	276.744083	-33.730270	14.129	13.516	13.358	-64.671	4530				
402	276.879971	-33.675831	14.138	13.436	13.357	13.679	4500				
403	276.873784	-33.655762	14.143	13.553	13.461	181.139	4785				
404	276.750878	-33.678814	14.145	13.559	13.397	-16.703	4593				
406	276.773448	-33.816742	14.159	13.602	13.453	89.280	4713				
407	276.538950	-33.857552	14.167	13.626	13.426	-59.382	4617				
408	276.702749	-33.817944	14.168	13.557	13.489	-91.236	4797				
409	276.578957	-33.705822	14.171	13.622	13.446	0.475	4665				
410	276.753490	-33.738415	14.173	13.552	13.448	24.100	4659				
411	276.836391	-33.686768	14.174	13.593	13.453	21.788	4669				
412	276.501238	-33.637436	14.174	13.595	13.412	-161.418	4563				
413	276.662487	-33.626492	14.179	13.651	13.492	50.701	4778				
414	276.628673	-33.566936	14.185	13.516	13.421	-5.715	4555				
415	276.534514	-33.915627	14.195	13.583	13.469	58.092	4660				
416	276.673953	-33.712120	14.197	13.610	13.502	-111.533	4751				
417	276.561145	-33.898586	14.197	13.540	13.448	47.080	4592				
419	276.578991	-33.573586	14.206	13.587	13.472	-41.636	4641				
420	276.687936	-33.576183	14.212	13.551	13.441	-69.762	4535	2.5	+0.05	0.5	*
422	276.852338	-33.874542	14.215	13.578	13.489	-20.986	4650				
423	276.852706	-33.851723	14.232	13.667	13.550	45.436	4782				
424	276.886130	-33.787621	14.234	13.670	13.553	101.421	4785				
425	276.661265	-33.711018	14.238	13.657	13.487	23.665	4587				

Table 1. Continued.

No.	RA(J2000) deg.	Dec(J2000) deg.	<i>J</i>	<i>H</i>	<i>K</i>	RV km s ⁻¹	<i>T</i> _{eff} K	log <i>g</i>	[M/H]	log ϵ (Li)	FG
(1)	(2)	(3)	(4)	(5)	(6)	(7)	(8)	(9)	(10)	(11)	(12)
426	276.616342	-33.801567	14.238	13.734	13.527	-107.099	4704				
427	276.858769	-33.890724	14.238	13.579	13.486	-152.559	4575				
428	276.683750	-33.836472	14.242	13.685	13.528	-70.446	4692				
429	276.794492	-33.592255	14.245	13.644	13.565	3.931	4796				
430	276.767692	-33.907009	14.247	13.673	13.511	-154.454	4622				
431	276.561013	-33.621979	14.248	13.682	13.531	82.186	4692				*
433	276.801658	-33.837830	14.256	13.632	13.536	-60.959	4670				*
434	276.665024	-33.724117	14.258	13.665	13.550	-22.264	4713				*
435	276.768679	-33.857334	14.259	13.664	13.559	99.095	4730				
436	276.493553	-33.646214	14.263	13.713	13.588	-50.196	4822				*
437	276.827726	-33.647717	14.268	13.643	13.542	-52.388	4655				
438	276.594804	-33.845116	14.271	13.742	13.515	5.719	4573				
440	276.631808	-33.564571	14.278	13.711	13.603	14.329	4819				
441	276.700830	-33.637337	14.281	13.799	13.534	-18.383	4598				
443	276.727795	-33.730831	14.297	13.769	13.573	-32.104	4663				
445	276.472846	-33.808666	14.310	13.670	13.574	73.543	4634	2.6	+0.25	0.7	
446	276.438307	-33.774590	14.311	13.721	13.542	-8.678	4544				
447	276.777476	-33.775871	14.316	13.739	13.634	-81.331	4786				
448	276.706230	-33.843826	14.316	13.735	13.588	-20.233	4649				
449	276.798371	-33.735714	14.320	13.855	13.631	5.772	4765				
451	276.887413	-33.852146	14.324	13.738	13.636	-184.313	4762	2.6	-1.05	0.8	
452	276.661034	-33.891323	14.334	13.821	13.654	-76.626	4794	2.6	-0.99	0.7	
453	276.690616	-33.808006	14.336	13.754	13.596	-48.148	4615				
454	276.698507	-33.939789	14.343	13.800	13.657	115.364	4773				
455	276.845583	-33.661392	14.344	13.746	13.667	65.842	4802				
456	276.593340	-33.672127	14.349	13.759	13.642	-23.056	4719				
457	276.833423	-33.746063	14.353	13.767	13.581	-23.375	4524				
459	276.615328	-33.576347	14.368	13.740	13.606	49.302	4561				
460	276.722855	-33.943268	14.391	13.838	13.708	-73.249	4781				
461	276.834942	-33.635342	14.396	13.863	13.666	-19.355	4643	2.7	-1.50	0.8	
462	276.789630	-33.841022	14.400	13.855	13.727	4.985	4813				
463	276.467867	-33.749195	14.400	13.783	13.650	-172.922	4595				
464	276.657623	-33.651539	14.406	13.786	13.632	-66.065	4526				
465	276.631871	-33.704411	14.417	13.879	13.739	-121.778	4806				
466	276.861515	-33.729511	14.417	13.903	13.742	-59.983	4806				
467	276.742712	-33.819698	14.422	13.889	13.745	-9.504	4802				
468	276.511268	-33.792122	14.422	13.791	13.707	56.092	4696				
469	276.581345	-33.660347	14.425	13.834	13.711	-44.438	4699				
471	276.439088	-33.761520	14.447	13.839	13.738	35.018	4717				
472	276.823834	-33.629124	14.464	13.925	13.731	131.626	4635				
473	276.670917	-33.612740	14.466	13.942	13.796	24.364	4833				*
474	276.547004	-33.669544	14.475	13.910	13.772	-17.630	4733				
476	276.661846	-33.655987	14.491	13.900	13.829	-29.627	4859				
477	276.853016	-33.748569	14.496	13.867	13.809	-75.148	4768	2.7	-1.09	0.7	
478	276.533779	-33.846905	14.501	13.982	13.812	-38.002	4772				
481	276.777363	-33.671219	14.502	13.896	13.736	-11.567	4543				*
482	276.573957	-33.858578	14.505	14.030	13.800	-154.032	4722	2.7	-0.78	0.9	
483	276.603613	-33.823669	14.506	13.932	13.766	31.359	4618				
484	276.594676	-33.571365	14.507	13.849	13.829	-6.386	4810				*
485	276.530138	-33.766701	14.511	13.876	13.792	129.335	4684				
486	276.865712	-33.679306	14.515	13.996	13.838	-56.181	4801				
487	276.849420	-33.771736	14.519	13.847	13.786	-141.982	4631				
488	276.598639	-33.744186	14.521	13.967	13.832	-3.129	4771				
489	276.875366	-33.742172	14.521	13.810	13.769	73.034	4577				
490	276.712242	-33.794239	14.531	13.928	13.856	-2.514	4810				
491	276.751951	-33.710484	14.534	13.883	13.786	-47.811	4593				
493	276.631945	-33.662464	14.538	13.956	13.862	54.638	4813	2.7	-1.12	0.9	*
494	276.572343	-33.570671	14.542	13.939	13.812	-28.906	4653				
495	276.548845	-33.833427	14.549	13.924	13.793	34.963	4575				
496	276.765063	-33.868202	14.555	13.990	13.859	77.859	4742				
497	276.830924	-33.896267	14.555	13.988	13.816	-30.904	4612				
498	276.771491	-33.669971	14.559	13.951	13.817	-23.933	4610				
499	276.633311	-33.762764	14.567	13.899	13.838	31.087	4650				
500	276.602649	-33.731819	14.567	14.041	13.883	-1.571	4787				
501	276.858813	-33.772926	14.568	13.883	13.878	174.776	4759				

Table 1. Continued.

No.	RA(J2000) deg.	Dec(J2000) deg.	J	H	K	RV km s ⁻¹	T_{eff} K	log g	[M/H]	log $\epsilon(\text{Li})$	FG
(1)	(2)	(3)	(4)	(5)	(6)	(7)	(8)	(9)	(10)	(11)	(12)
503	276.436893	-33.808731	14.580	13.968	13.852	-36.423	4659				
504	276.481768	-33.625542	14.581	13.971	13.872	-67.245	4718				
505	276.537031	-33.778503	14.584	14.036	13.893	-9.908	4767				
506	276.502711	-33.686172	14.585	13.967	13.838	-10.462	4604				
507	276.736185	-33.691521	14.591	13.961	13.833	-87.751	4566				
508	276.761504	-33.739830	14.594	13.971	13.862	-231.533	4638	2.7	-0.71	0.9	
509	276.856836	-33.670521	14.596	13.998	13.898	-150.306	4737	2.7	-0.76	0.7	
511	276.586662	-33.710934	14.606	13.974	13.869	106.628	4629				
512	276.620755	-33.646839	14.620	14.124	13.932	-19.865	4776				
513	276.868502	-33.816536	14.620	14.136	13.959	39.173	4851				
514	276.727030	-33.799290	14.624	14.014	13.922	42.665	4727				*

Notes. Meaning of the columns: (1): Target number in this programme; (2): Right ascension from 2MASS; (3): Declination from 2MASS; (4), (5), and (6): 2MASS J -, H -, and K -magnitude; (7): Heliocentric radial velocity; (8): Effective temperature; (9): Surface gravity log g ; (10): Metallicity; (11): Li abundance; (12): Flag for foreground stars.